Proceedings of the 4th International Conference on Machine Learning and Automation
DOI: 10.54254/2755-2721/2026.38046

Force Feedback and Force Sensing in Humanoid Robotic Arm Structures

Chenjia Li

Moreau Catholic High School, Hayward, USA
lcj20070909@gmail.com

Abstract. Humanoid robotic arms must manage uncertain contact during grasping, assembly, transport, and physical human-robot interaction. Vision and high-gain position control provide useful pre-contact geometry but cannot continuously reveal contact location, force direction, shear, slip, or load variation. This paper examines how force information is generated, transmitted, measured, and fed back through five actuation routes: high-gear-ratio rigid drives, series elastic actuators, variable-stiffness actuators, low-gear-ratio quasi-direct drives, and cable remote drives. Joint torque sensing, wrist six-axis force/torque sensing, and distributed tactile sensing are compared as complementary layers. The synthesis shows that interaction performance depends jointly on reflected inertia, structural stiffness, elastic elements, load paths, calibration quality, and control bandwidth. Sensor placement, overload protection, compliance, thermal management, and maintenance access therefore belong to one structural design problem rather than an afterthought. The paper provides a traceable framework for selecting sensing locations and actuation structures and identifies range, calibration, overload recovery, bandwidth, and serviceability as validation targets for future hardware experiments.

Keywords: Humanoid robotics, robotic arm, force feedback, force sensing, compliant actuation

1. Introduction

Humanoid robotic arms operate in tasks where the intended motion is only partly known before contact. During grasping, object mass, friction, and center of mass can vary. During insertion, a small alignment error can create a large lateral force at the tool. During transport and physical human-robot interaction (pHRI), the forearm, hand dorsum, or upper-arm surface can also become a contact interface. Vision supplies geometry and target pose before contact, but it does not replace pressure, shear, slip, or material-compliance information [1]. A structure that only maximizes position stiffness can convert a small pose error into a damaging contact impulse. A practical arm therefore needs controlled deformation, overload bypass paths, and sensing locations that preserve the meaning of the measured load.

Force sensing estimates external force, joint torque, or contact distribution, whereas force feedback feeds those estimates into a closed loop that changes joint torque, end-effector pose, or desired impedance. Impedance control describes the desired mass, damping, and stiffness

© 2026 The Authors. This is an open access article distributed under the terms of the Creative Commons Attribution License 4.0 (https://creativecommons.org/licenses/by/4.0/).

DOI: 10.54254/2755-2721/2026.38046

relationship between a robot and its environment [2]. A passivity-based framework places position, torque, and impedance control in one energy-aware view and shows why joint flexibility, energy exchange, and communication delay affect contact stability [3]. Force feedback is therefore not a sensor added beside position control. It is a reorganization of the information path: calibration, temperature and gravity compensation, filtering, coordinate transformation, and limiting must produce a credible force state before the controller generates a correction.

From the hardware perspective, power density, gear ratio, reflected inertia, heat rejection, and serviceability must be considered together. A hardware review of humanoid platforms emphasizes the coupled effect of actuator packaging, transmission, and thermal constraints [4]. This paper asks how a robotic arm should select sensing locations, actuation structures, and feedback strategies so that force information enters the loop stably and becomes a verifiable interaction behavior. The analysis first defines measurement targets and the processing path. It then compares strain-based, capacitive, and multi-axis sensing constraints, followed by a comparison of compliant, quasi-direct, and remote-transmission actuation. The final section assigns distinct roles to wrist sensing, gripper touch, and contact skin. The contribution is a design review rather than an unvalidated arm proposal.

2. Force sensing foundations and structural constraints

2.1. Measurement targets and force information loop

The quantity reported by a force sensor depends on its location in the load path. A wrist-mounted six-axis force/torque (F/T) sensor normally outputs a wrench vector. A joint torque sensor is closer to the transmission chain, while a tactile array reports contact location and pressure distribution. These information types have different responsibilities in a closed loop. Proprioceptive signals from encoders, motor current, or spring deflection describe the robot state. Wrist F/T, tactile skin, and collision sensors describe environmental action more directly. Vision and tactile sensing are complementary in contact-rich manipulation [1]. The wrench vector is defined in Equation (1).

$$w = [F_x, F_y, F_z, M_x, M_y, M_z]^T \tag{1}$$

where F_x, F_y, and F_z are force components and M_x, M_y, and M_z are moment components.

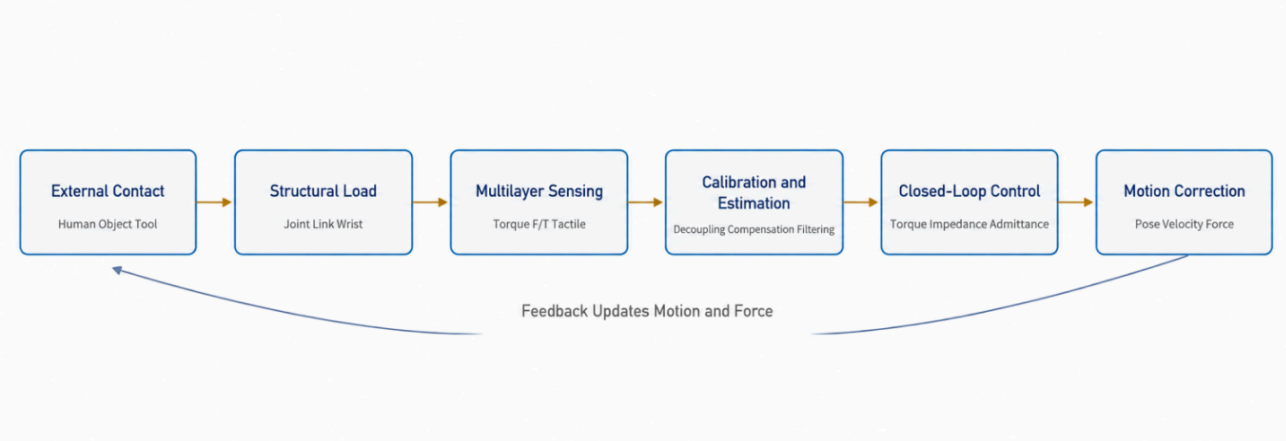

Figure 1. Force feedback loop (picture credit: original)

DOI: 10.54254/2755-2721/2026.38046

The raw electrical signal cannot be sent directly to a controller. Amplification, calibration, temperature and gravity compensation, filtering, frame transformation, and saturation define the usable force state. Motor-current torque estimates are inexpensive but include gear friction, temperature, and transmission-efficiency errors. Output-side strain or spring displacement adds mechanical complexity but avoids part of the motor-side uncertainty. Backlash creates a dead zone, an overly soft elastic element lowers the natural frequency, and communication delay can excite contact oscillation. The complete path is summarized in Figure 1.

2.2. Force sensors and sensing principles

Strain-based sensing is a common route for joint torque and multi-axis F/T measurement. A loaded elastic body produces strain, and the relative resistance change of a strain gauge is approximately proportional to strain through the gauge factor G. Strain gauges are placed on designed beams and commonly connected as a Wheatstone bridge to increase the useful signal and reject part of the temperature variation. The structural objective is to create repeatable strain in a measurable region while keeping bearing loads and overloads out of the measurement beam. The resistance relation is given in Equation (2).

$$\frac{\Delta R}{R} = G\varepsilon \tag{2}$$

where ΔR/R is the relative resistance change, G is the gauge factor, and ε is strain.

Scalable strain-gauge joint torque sensing has linked elastic-body geometry, strain concentration, and assembly to the load path [5]. A six-axis wrist sensor design maps different load directions to dedicated beams and multiple strain channels, showing that multi-axis measurement is first a structural decoupling problem and only then an electrical readout problem [6]. A beam that is too thick suppresses signal, while a beam that is too thin sacrifices stiffness, natural frequency, and overload capacity. The strain route therefore uses local, controlled compliance while retaining stiffness in the primary load-bearing structure.

Capacitive sensing measures force through a change in electrode overlap area A, spacing d, or dielectric permittivity. The approach is suitable for thin sensing units in tight spaces. A coin-sized capacitive six-axis sensor demonstrates the compact form factor, but hysteresis, thermal drift, and nonlinear response from the elastic support and dielectric layers still require calibration [7]. Size alone is not a sufficient selection criterion. Stability over the working range, package reliability, and calibration maintenance must also be compared. The capacitance relation is given in Equation (3).

$$C = \frac{\varepsilon A}{d} \tag{3}$$

where *C is capacitance, ε is permittivity, A is electrode overlap area, and d is electrode spacing.*

Multi-axis sensors must keep cross-axis coupling within a correctable range. Symmetric beams, crossed beams, and local decoupling structures can make one load direction dominate a specific measurement region. Flange flatness, bolt preload, cable pull, and installed pose nevertheless alter the sensitivity matrix. In-situ nonlinear calibration of humanoid force/torque sensors shows that factory calibration cannot replace multi-direction loading and gravity compensation after installation [8]. The surrounding structure should therefore provide repeatable loading access, removable interfaces, and mechanical limits or bypasses that protect the elastic body. These sensing layers and structural requirements are summarized in Table 1.

DOI: 10.54254/2755-2721/2026.38046

Table 1. Sensing layers and structural requirements

Location	Measured quantity	Strength	Limitation	Structural focus
Motor side	Estimated torque	Low cost	Friction error	Low friction
Joint output	Joint torque	Fast inner loop	External-force separation	Strain concentration
Wrist	Six-axis wrench	Tool contact	Link blind spots	Rigid flange
Link or skin	Contact distribution	Body coverage	Drift and wiring	Modular package
Fingertip or gripper	Local force	Slip cues	Wear exposure	Wear-resistant stop

2.3. Force control and feedback mechanisms

Impedance control specifies how a robot should respond to external force rather than requiring a single exact position. The desired inertia, damping, and stiffness appear in the impedance relation, and the end-effector wrench is mapped to joint torque through the Jacobian. These relations are expressed in Equations (4) and (5). A low-friction arm with direct torque control can use pose error to generate the torque required for a target impedance. A platform with a stiff internal position loop more commonly uses admittance control: the measured external force is converted to a pose or velocity correction for the inner loop.

$$M_d\,\ddot{x} + D_d\,\dot{x} + K_d(x - x_d) = F_{ext} \tag{4}$$

where *M_d, D_d, and K_d are desired inertia, damping, and stiffness; x_d is desired pose; and F_ext is external force.*

$$\tau = J^T F \tag{5}$$

where *J is the task Jacobian, F is the end-effector wrench, and τ is the joint torque.*

The two routes share the goal of shaping contact dynamics but differ in where force information enters the loop and whether the mechanics can execute the desired torque. A passivity-based treatment of flexible-joint robots emphasizes that the controller should limit net energy delivered to an unknown environment [3]. High gear reduction and friction increase the delay pressure on an outer admittance loop. Measurable elasticity, output torque sensing, and low reflected inertia shorten the path from contact to the inner control action.

2.4. Sensing-driven structural design

Sensor location determines directness and interpretability. Motor-current estimation is easy to integrate but mixes transmission uncertainty into the estimate. Output-side joint torque is better suited to a high-frequency inner loop and whole-arm collision estimation. Wrist six-axis F/T describes the net tool wrench, while link and skin tactile sensing add contact location and pressure distribution. The layers are not redundant: the joint layer indicates where an abnormal torque enters

DOI: 10.54254/2755-2721/2026.38046

the transmission, the wrist layer describes net tool interaction, and the outer layer localizes body contact.

A sensor cannot be attached after the arm has been structurally frozen. The elastic body must place useful strain in a defined region while bearings, flanges, and bypass members isolate unrelated loads. Normal, impact, and overload paths should be separated before the sensor geometry is fixed. Assembly must then support multi-direction loading and in-situ calibration. Mechanical compliance and active compliance solve adjacent problems. Series or variable-stiffness structures absorb part of an impact before the controller responds, low gear reduction improves backdrivability through lower reflected inertia, and rigid high-reduction structures depend more on sensing, collision detection, and outer-loop correction.

Compliance is not maximized by making the spring as soft as possible. Excessively soft elements produce static sag, pose error, and low-frequency vibration. Excessively stiff elements reduce small-force resolution and energy absorption. The target stiffness should follow maximum load, allowable deflection, task frequency, and required force bandwidth. Mechanical limits, overload channels, speed-dependent thresholds, temperature monitoring, and fault shutdown are part of the safety structure. A useful arm combines local measurable compliance with global load-bearing stiffness and evaluates cross-talk, hysteresis, thermal drift, natural frequency, overload recovery, and fatigue life.

Lightweight design is also a decision about where mass is placed. Moving motors and drives toward the shoulder reduces distal inertia but adds transmission, heat, and maintenance constraints. Expanding the tactile skin increases connectors, communication nodes, and service points. Structure, sensing, and electrical packaging should therefore be planned together from the concept stage. Flexible tactile skin research further shows that sensor geometry must be calibrated in the robot frame when a sheet is wrapped over a curved surface.

3. Robotic arm architecture and key components

3.1. Degrees of freedom, links, and transmission topology

The degrees of freedom (DOF) of a humanoid upper limb should serve posture adjustment, obstacle avoidance, manipulability, and contact-force allocation rather than mechanically copying the human arm. A seven-DOF arm adds one redundancy to the six-DOF end-effector pose and can change elbow posture without changing the task pose. The redundancy also adds a motor, bearing, encoder, cable, and maintenance burden. DOF count should follow task space, load, and service constraints.

Link and transmission topology determine distal inertia and sensing quality. Placing motors, reducers, and drives near the base usually lowers moving mass and collision energy. Primary links should carry bending and torsion, while non-load-bearing covers can remain light and removable and provide space for tactile modules, wiring, and cooling. Modular joints should specify axial and radial load paths, hard stops, zero calibration, and quick-change interfaces so that the sensor is not forced to carry a bearing load.

A conventional serial joint is modular but moves motor mass with the link. A cable remote drive moves heavy components toward the torso or shoulder at the cost of cable stretch, pulley friction, and changing pretension. D3-ARM demonstrates a high-dynamic, lightweight, and decoupled cable-driven arm with base-mounted electrical components [9]. Distal mass reduction should be evaluated with dual encoders or tension estimation, pretension retention, and maintenance frequency rather than by mass alone.

DOI: 10.54254/2755-2721/2026.38046

3.2. Actuation systems and joint modules

The reflected rotor inertia rises with the square of the gear ratio, as shown in Equation (6). A larger ratio increases output torque and static holding ability but makes external force less able to back-drive the motor and magnifies the effects of friction and backlash. The equation captures why actuation routes differ in contact transparency.

$$J_{ref} = N^2 J_m \tag{6}$$

where *J_ref is reflected rotor inertia, N is gear ratio, and J_m is motor rotor inertia.*

High-gear-ratio rigid joints target load capacity and mature engineering implementation. They commonly combine wrist F/T sensing with outer-loop admittance to obtain limited compliance, but the response remains delayed after a collision. Series elastic actuators add a measurable spring between motor and load. Low-gear-ratio or quasi-direct-drive actuators use low friction and low reflected inertia to improve backdrivability. These routes improve contact behavior through different mechanisms: passive buffering in the first case and fast active torque control in the second.

Series elastic actuation uses spring deflection as output torque information and provides both force feedback and impact buffering [10]. A variable-stiffness actuator review connects stiffness range, output power, potential energy, efficiency, accuracy, sensor setup, and control design [11]. Proprioceptive actuation for dynamic robots further links low reflected inertia and impact mitigation to high-bandwidth physical interaction [12]. The spring relation is given in Equation (7). A spring that is too soft increases pose error and reduces force bandwidth, while a spring that is too stiff reduces force resolution and energy absorption. Variable stiffness changes pretension or geometry to switch between soft contact and fast motion, but the added mechanism increases mass, size, and control state.

$$\tau = k_s \delta \tag{7}$$

where *τ is output torque, k_s is spring stiffness, and δ is relative spring deflection.*

No actuator route is optimal for every task. Shoulder and elbow joints that carry sustained load may prioritize continuous torque, thermal capacity, and output torque observability. Distal joints are more constrained by mass, backdrivability, and installation space. The design process should define maximum load, allowable deflection, contact frequency, and maintenance conditions before choosing rigid, elastic, low-reduction, or remote transmission. Figure 2 compares the actuation pathways, and Table 2 summarizes their design trade-offs.



Figure 2. Actuation pathways (picture credit: original)

DOI: 10.54254/2755-2721/2026.38046

Table 2. Actuation trade-offs

Actuation route	Backdrivability	Buffering	Strength	Cost
High-gear-ratio rigid	Low	Control	High load	Friction and backlash
Series elastic	High	Spring	Torque sensing	Pose error
Variable stiffness	Adjustable	Stiffness change	Range control	Complex structure
Quasi-direct drive	High	Low inertia	High bandwidth	Thermal management
Cable remote drive	Variable	Cable compliance	Low distal mass	Friction and service

3.3. Wrist, gripper, and contact skin

A wrist six-axis F/T sensor outputs the net wrench between tool and environment rather than a single force direction. The three force components describe the resultant force, and the three moment components describe the effect of the load about the sensor origin. The sensor is therefore useful for precise tool force, gravity compensation, and contact-state estimation, but it cannot directly distribute force among multiple fingertip contacts. The primary structural requirement is a clear and stiff load path that forces normal tool loads through the sensing elastic body instead of allowing them to bypass it.

A common end-effector layout places a rigid interface between the last wrist joint and the tool flange and locates the six-axis sensor near that interface. The arrangement continues to measure the net wrench after a gripper or tool is exchanged, but the sensor can become a local compliance bottleneck and tool mass and center of mass introduce attitude-dependent gravity terms. Center-of-mass-based grasp pose adaptation combines 3D range with force/torque sensing to add contact constraints that vision alone cannot provide [13].

Soft tactile upper-body research shows that compliant coverings can expand the usable body-contact area for large-object manipulation and physical interaction [14]. The result does not mean that more coverage is always better. Soft materials change local geometry and load transfer and add wiring, cleaning, aging, and repair requirements. Link and hand surfaces are better served by small replaceable tactile modules, common connectors, and removable soft covers over a rigid skeleton with controlled compression space.

Recent work on contact-force estimation models transmission friction and uncertain torque without requiring a dedicated F/T sensor, which reinforces the need to characterize the load path and model uncertainty [15]. A flexible tactile skin integration study shows that spatial calibration can map curved sensor cells into the robot frame for controller input [16]. An integrated tactile system for humanoid grasping closes the loop from pressure sensing through data acquisition to a threshold-based stop command [17]. Together, these results support a three-layer division: the wrist provides net tool wrench, the gripper provides local grip and slip cues, and the outer skin provides non-terminal contact location and pressure distribution.

4. Conclusion

Humanoid robotic arms entering real contact environments cannot rely on vision and position control alone to handle object variation, friction changes, accidental collision, and multi-point loading. The value of force sensing is not only a numerical measurement. It is the ability to identify where an external load enters the structure, which components carry it, and how it should change

DOI: 10.54254/2755-2721/2026.38046

motion. Output-side joint torque sensing, wrist six-axis F/T sensing, and distributed tactile sensing serve transmission anomaly detection, net tool wrench estimation, and contact localization respectively. Consistent time stamps, coordinate calibration, and a safety state machine are required to turn these signals into one closed loop.

Actuation routes have no task-independent ranking. High-gear-ratio rigid joints support sustained load and mature implementation but have weak backdrivability. Series elastic actuators trade measurable compliance for impact buffering and force-control conditions. Variable-stiffness actuators widen the adjustable range but add mechanism and control complexity. Low-gear-ratio actuators support high-bandwidth interaction but face motor-size, heat-rejection, and continuous-torque limits. Cable remote drives reduce distal mass but require friction, pretension, and service management. Maximum load, allowable deflection, and task frequency should be defined before an arm selects a transmission.

The synthesis indicates that sensing and structure should be designed from the same load path. Local controlled compliance can create a calibratable signal while the primary load-bearing structure retains stiffness. Mechanical stops, overload bypasses, thermal management, cable routing, and service interfaces form a safety boundary outside software. Future experiments should quantify these trade-offs at component, joint, and whole-arm levels under explicit range, bandwidth, calibration, and risk limits. The present paper is a literature-based structural audit framework. Each sensing layer should be paired with a defined load path, calibration condition, overload protection method, and maintenance interface before a specific task claim is made.

References

[1] Dahiya, R. S., Metta, G., Valle, M., & Sandini, G. (2010). Tactile sensing - From humans to humanoids. *IEEE Transactions on Robotics, 26*(1), 1–20.

[2] Hogan, N. (1985). Impedance control: An approach to manipulation: Part I - Theory. *Journal of Dynamic Systems, Measurement, and Control, 107*(1), 1–7.

[3] Albu-Schaffer, A., Ott, C., Frese, U., & Hirzinger, G. (2007). A unified passivity-based control framework for position, torque and impedance control of flexible joint robots. *International Journal of Robotics Research, 26*(1), 23–39.

[4] Ficht, G., & Behnke, S. (2021). Bipedal humanoid hardware design: A technology review. *Current Robotics Reports, 2*, 201–210.

[5] Khan, H., et al. (2017). Towards scalable strain gauge-based joint torque sensors. *Sensors, 17*(8), Article 1905.

[6] Hu, S., Wang, H., Wang, Y., & Liu, Z. (2018). Design of a novel six-axis wrist force sensor. *Sensors, 18*(9), Article 3120.

[7] Choi, H., et al. (2025). CoinFT: A coin-sized, capacitive 6-axis force torque sensor for robotic applications. arXiv:2503.19225.

[8] Mohamed, H. A. O., et al. (2023). Nonlinear in-situ calibration of strain-gauge force/torque sensors for humanoid robots. In *Proceedings of the IEEE-RAS International Conference on Humanoid Robots*, pp. 1–8.

[9] Luo, H., Xu, J., Li, S., Liang, H., Chen, Y., Xia, C., & Wang, X. (2025). D3-ARM: High-dynamic, dexterous and fully decoupled cable-driven robotic arm. arXiv:2502.12963.

[10] Pratt, G. A., & Williamson, M. M. (1995). Series elastic actuators. In *Proceedings of the IEEE/RSJ International Conference on Intelligent Robots and Systems*, pp. 399–406.

[11] Wolf, S., et al. (2016). Variable stiffness actuators: Review on design and components. *IEEE/ASME Transactions on Mechatronics, 21*(5), 2418–2430.

[12] Wensing, P. M., et al. (2017). Proprioceptive actuator design in the MIT Cheetah: Impact mitigation and high-bandwidth physical interaction for dynamic legged robots. *IEEE Transactions on Robotics, 33*(3), 509–522.

[13] Kanoulas, D., et al. (2018). Center-of-mass-based grasp pose adaptation using 3D range and force/torque sensing. *International Journal of Humanoid Robotics, 15*, Article 1850017.

[14] Goncalves, A., Kuppuswamy, N., Beaulieu, A., Uttamchandani, A., Tsui, K. M., & Alspach, A. (2022). Punyo-1: Soft tactile-sensing upper-body robot for large object manipulation and physical human-robot interaction. In

DOI: 10.54254/2755-2721/2026.38046

Proceedings of the IEEE 5th International Conference on Soft Robotics, pp. 1–8.
[15] Wang, Y., et al. (2024). Contact force estimation using uncertain torque model and friction models for robot manipulator. *IEEE Transactions on Industrial Electronics, 71*(10), 12634–12644.
[16] Chefchaouni Moussaoui, S., et al. (2023). Spatial calibration of humanoid robot flexible tactile skin for human-robot interaction. *Sensors, 23*(9), Article 4569.
[17] Bao, R., et al. (2023). Integrated intelligent tactile system for a humanoid robot. *Science Bulletin, 68*(10), 1027–1037.